Solvent Penetration and Photoresist Dissolution: A Fluorescence Quenching and Interferometry Study

WILLIAM LIMM, DEIRDRE STANTON, GERALD P. DIMNIK, and MITCHELL A. WINNIK, *Department of Chemistry and Erindale College, University of Toronto, Toronto, Ontario M5S 1A1 Canada,* and BARTON A. SMITH, *IBM Research Division, Almaden Research Center, San Jose, California 95120-6099*

Synopsis

A novel method, based upon fluorescence quenching measurements, is described for the study of the mechanistic details of solvent penetration into thin polymer films. Here poly(methyl methacrylate) (PMMA) labelled with phenanthrene (Phe) groups was coated as a film (0.8 μm thick) onto quartz disks. Diffusion of solvent (1 : 1 2-butanone/2-propanol) into the film was followed by a decrease in Phe fluorescence, while film dissolution was monitored simultaneously by laser interferometry. In the case of PMMA (M_w = 411,000, films annealed at 160°C) both processes occur at approximately the same rate and exhibit non-Fickian (relaxation-controlled) diffusion behavior. Correlating the results of these two experiments shows that, once the steady state is reached, the dissolution rate is controlled by the advance of the solvent front into the PMMA film. The "transition layer," an important dissolution parameter, increases its thickness from 50 to 90 nm during the plasticization stage of solvent penetration and maintains its thickness until the solvent front reaches the quartz substrate.

INTRODUCTION

A new method for studying the fundamental details of photoresist dissolution based upon a fluorescence quenching technique is introduced. In this method, the photoresist polymer is labeled with a small amount of a fluorescent dye whose fluorescence is quenched by the solvent used to dissolve the film. When the film is exposed to solvent, fluorescence from the dye decreases with time. Loss of fluorescence is due to two effects: (i) diffusion of the solvent molecules into the film which leads to fluorescence quenching and (ii) dissolution of the polymer. Normally, only the latter process is measured.[1] Here we demonstrate that the rates of both processes can be measured simultaneously. We use a flow cell equipped with a fiber-optic device to measure film thickness changes via laser interferometry. This cell is mounted in the sample compartment of a standard fluorescence spectrometer allowing simultaneous monitoring of the time profiles of film thickness and the fluorescence intensity of the dye bound to the polymer film.

Experiments described here pertain to poly(methyl metacrylate) (PMMA) films. PMMA is unusual in that it has virtually perfect dissolution characteristics for a photoresist material. Under normal processing conditions it dissolves without noticeable swelling, thus providing very high resolution in the exposure and development processes. In such a material it is likely that

Journal of Applied Polymer Science, Vol. 35, 2099–2116 (1988)
© 1988 John Wiley & Sons, Inc. CCC 0021-8995/88/082099-18$04.00

solvent penetration is the rate limiting step in film dissolution. Our experiments, which allow one to follow solvent penetration directly, largely confirm this point of view.

We examine the dissolution of thin PMMA films in a 1 : 1 mixture of 2-butanone and 2-propanol (1 : 1 MEK/IPA). By carrying out both measurements simultaneously, we are able to obtain new insights into the dissolution process. We can show, for example, that once the steady state is reached, the dissolution rate is controlled by the advance of the solvent front into the PMMA film. In addition, the "transition layer," a dynamic dissolution layer that is sandwiched by bulk solvent and solid polymer film, exhibits an interesting behavior. Its thickness increases from 50 to 90 nm exclusively during the plasticization stage of solvent penetration and, thereafter, maintains its thickness until the solvent front reaches the quartz substrate.

BACKGROUND

Polymer Dissolution

Phenomenological studies of the dissolution of amorphous glassy polymers upon exposure to solvent date back more than 30 years. A modern understanding of thin polymer film dissolution, pertinent to the application of these films as photoresists, owes much to the work of Ouano and his co-workers[2-4] at IBM.

From a mechanistic point of view, the process of polymer dissolution can be divided into three major steps. The first is the diffusion of solvent molecules into a rigid polymer matrix driven by a chemical potential gradient. The second step is the solvation and swelling of the polymer network resulting in the formation of a gel layer between the solvent and the glassy film. This process, which is sometimes referred to as plasticization, enables segmental motion of the polymer chain to commence. This, in turn, increases the mobility of solvent molecules in the polymer network resulting in acceleration of solvent penetration. The final step of polymer dissolution is the separation of a polymer molecule from the network and its diffusion into the bulk solvent.

If the polymer matrix does not offer much resistance to the diffusing solvent molecules, as in the case of a rubbery polymer, the first step (diffusion of solvent molecules) controls the diffusion rate. This is classical "random-walk" diffusion, and can be described by Fick's law.[5] On the other hand, if the polymer matrix is glassy, it resists swelling, and the second step is rate-controlling. This is described by the relaxation-controlled diffusion model[6-8] (Case II diffusion), which is characterized by a well-defined solvent–polymer boundary propagating through the polymer network. If the rates of the first and the second steps are comparable, so-called "anomalous" diffusion[6] is expected.

The third step rarely determines the overall dissolution rate in itself, although there is some suggestion that the duration of this step could be manipulated.[9]

Fluorescence Quenching

An excited chromophore has various potential pathways for its relaxation to the ground state. The term "quenching" encompasses all bimolecular

processes that decrease the probability of radiative relaxation. There are many known quenching mechanisms with critical quenching distances ranging from 2 to 100 Å.[10]

Fluorescence quenching processes are divided into two major categories:[11] (1) static quenching which involves no mass diffusion and (2) dynamic quenching which involves mass diffusion of quencher and/or chromophore.

Quenching observed in rigid media is normally attributed to static quenching. The active sphere model[12] is used to determine static quenching parameters. In this model, an imaginary sphere is defined with an excited chromophore at its center. If a quencher molecule is present within this sphere, quenching occurs instantaneously. If no quencher is present within this sphere, no quenching occurs. From this simple model, one can derive the expression

$$I_0/I = \exp(c/c_0) \tag{1}$$

where I_0 and I are fluorescence intensities of chromophore in the presence and in the absence of a quencher, respectively, c is the quencher concentration, and $c_0 = 3/(4\pi N_A R_0^3)$, where N_A is Avogadro's number and R_0 is the radius of the quenching sphere.* Here we use steady state fluorescence data to show that phenanthrene quenching by ketones involves an R_0 on the order of 5 Å.

When solvent molecules diffuse into a polymer film, plasticization commences. This increases the mobility of Phe labels on PMMA as well as that of the solvent. Then, dynamic quenching may become the dominant quenching process. Under these conditions, the Phe fluorescence intensity is governed by the Stern–Volmer equation[14]

$$I_0/I = 1 + k_q\tau^0[\mathrm{Q}] \tag{2}$$

where [Q] is the quencher concentration, k_q is the quenching rate constant, and τ^0 is the lifetime of Phe fluorescence in the absence of a quencher. When quenching is diffusion-controlled,

$$k_q = 4\pi N_A R_0 D/1000 \tag{3}$$

where D is the sum of the diffusion constants of the diffusing species. At high polymer volume fraction, the magnitude of D is sensitive to the fraction of solvent in the mixture. An increase of ketone concentration within some region of the polymer film will not only decrease fluorescence through the [Q] term in eq. (2), but it will increase D and hence k_q as the polymer swells. Where Case II diffusion is prominent, one might expect to see the largest contribution to fluorescence quenching associated with the moving solvent front as it passes through the polymer.

We determined k_q for quenching of 9-phenanthrylmethyl pivalate[15] by 2-butanone in cyclohexane solvent. This system is taken as a reasonable model for the phenanthrene chromophore bound to the PMMA polymer. We mea-

*A more sophisticated approach was taken by Inokuti and Hirayama,[13] who incorporated a distance-dependent quenching rate constant.

sured $\tau^0 = 46$ ns for Phe and calculated $k_q = 7.3 \times 10^8 M^{-1}$ s^{-1}. Note that this k_q value is somewhat less than diffusion-controlled ($k_{\text{diff}} = 7 \times 10^9 M^{-1}$ s^{-1}) in cyclohexane. In the experiment reported here, the solvent (1:1 MEK/IPA) has a ketone concentration of 5.6M, and therefore, $I_0/I \approx 200$. As a consequence, when the labeled polymer is fully dissolved in this solvent, only a nominal amount ($\approx$ 0.5%) of the initial fluorescence intensity remains.

EXPERIMENTAL

Labeled PMMA Synthesis and Characterization

The PMMA samples were prepared by AIBN-initiated bulk copolymerization of inhibitor-free methyl methacrylate with 9-phenanthrylmethyl methacrylate to 35% conversion. The product was purified by multiple reprecipitation from methanol and was dried for 24 h at room temperature *in vacuo*. Gel permeation chromatography (GPC) was used to determine the molecular weights of the polymer based on PMMA standards (Polymer Laboratories). From the data analysis $M_w = 411{,}000$, $M_n = 197{,}000$ and $M_w/M_n = 2.08$ were obtained.

The extent of phenanthrene labelling (ca. 1 mol %) was determined from UV absorption measurements (Hewlett Packard Model 8451A spectrometer) using 9-phenanthrylmethyl pivalate ($\epsilon = 12{,}500$ at 296 nm) as a reference. A PMMA chain contains, therefore, an average of 20 phenanthrene groups.

Photoresist Spinning and Baking

The PMMA sample was dissolved in toluene to prepare a solution of 8% by weight PMMA, which was passed through a Millipore filtering system (0.2 μm pore size). A 1-in. diameter substrate, either a quartz disk or a silicon wafer, was spin-coated using a Headway Research photoresist spinner Model EC101. After spinning at 1200 rpm for 40 s, PMMA films were baked in a vacuum oven at 160°C for 60 min to remove the residual toluene and to anneal the PMMA films ($T_g = 105$°C for atactic PMMA[15]). The samples were then removed from the oven and allowed to cool to room temperature. Talystep, UV, and interferometry measurements were carried out to determine the thickness of the baked PMMA films.

Static Quenching Measurement

To determine the critical quenching distance for the phenanthrene–ketone system, PMMA labeled with phenanthrene was dissolved in toluene along with a ketone dopant and was spin-coated onto quartz disks. Cyclohexanone (BP = 156°C) was chosen as the quencher. The percentage cyclohexanone content of PMMA films was determined via gas chromatography (GC). Each PMMA film sample along with its quartz substrate was first accurately weighed and then immersed in ca. 1 mL of acetone which completely dissolved the sample. The solution was analyzed by GC for cyclohexanone with respect to an internal standard (naphthalene). The quartz disk was reweighed to determine the total weight of the sample.

UV-absorbance spectra of PMMA films were used to determine optical thicknesses of samples and the observed fluorescence intensities of PMMA films were corrected in the following manner:

$$I_{\text{corrected}} = I_{\text{observed}}[1 - 10^{-a'}]/[1 - 10^{-a}] \quad (4)$$

where a' and a are absorbances of the sample and the blank at 298 nm, respectively.

Flow-Cell Design

A solvent flow-through cell that allowed the simultaneous interferometric and fluorescence intensity monitoring was constructed[16] (Fig. 1). The cell consists of a brass housing, a Teflon insert, a film substrate, a fiber-optic cable housing, and a combination of O-rings. The teflon insert is used to guide the flow of solvent to and away from the sample substrate. A simple rotating piston pump (Fluid Metering Inc.) delivering 150 strokes/min is used to pump the solvent, typically at 2 mL/min. Increasing the flow rate to 20 mL/min had little influence on the dissolution rate. The cell housing is equipped with a constant temperature jacket and is thus capable of performing temperature-controlled experiments. All the penetration/dissolution experiments reported here have been performed at 21°C.

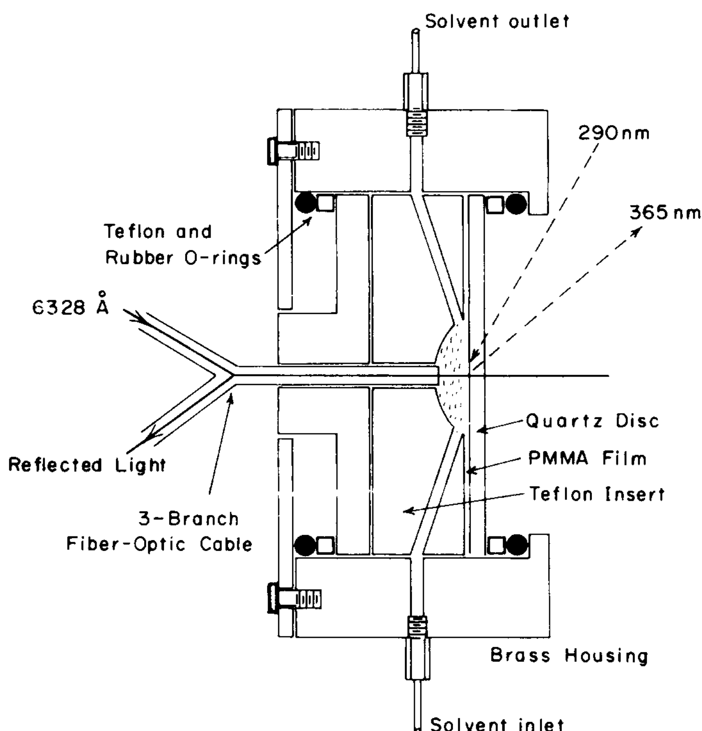

Fig. 1. The flow-cell design.

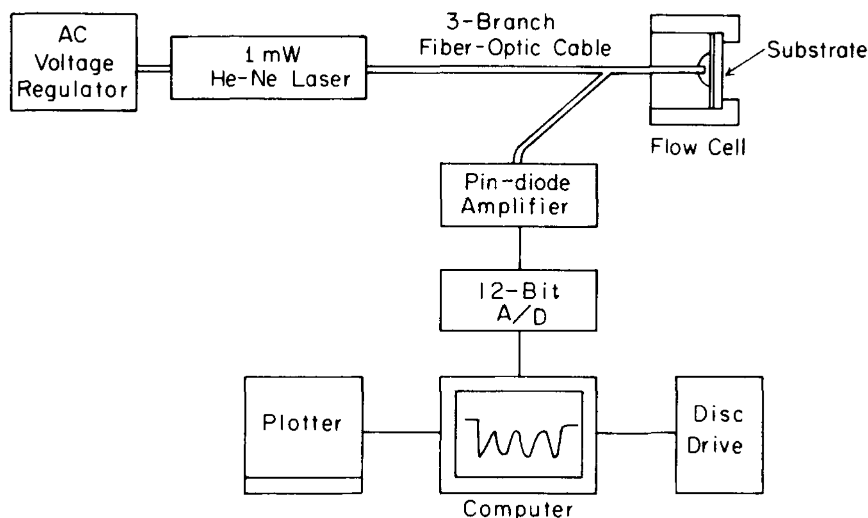

Fig. 2. The interferometry setup.

Interferometry

A simple laser interferometry technique† was utilized for this work. Figure 2 illustrates the optical arrangement. An unpolarized 6328 Å beam from a voltage-regulated helium–neon laser (Melles Griot, 1 mW) was directed at normal incidence via a randomized bifurcated fiber-optic cable (Dolan-Jenner Model ER824) to a PMMA film. For a normal incidence, the reflectivity R is given by the expression

$$R = \left[(n_1 - n_2)/(n_1 + n_2)\right]^2 \tag{5}$$

where n_1 and n_2 are indices of refraction of media 1 and 2, respectively. The index of refraction of a 1 : 1 MEK/IPA mixture by volume is approximately the numerical average of the indices of refraction of MEK (1.377) and IPA (1.375). The reflectivity calculated for the solvent/PMMA interface ($R_1 = 1.56 \times 10^{-3}$) indicates that a substantial amount of the He–Ne laser beam would be reflected at this interface. Provided that the reflectivity at the PMMA/substrate interface is sufficiently high, a moderately intense optical interference would occur.

This interference signal was carried through the same fiber-optic cable to the photodiode (United Detector Technology, PIN-10DP). The resulting voltage was amplified and relayed to an interface equipped with a 12-bit analogue-to-digital converter chip. For the dissolution of PMMA films spun on silicon wafers, the A/D interface was set for 10 V maximum, i.e., $2^{12} = 10$ V. For quartz samples, which produce weaker interference intensity, the interface was set at 2.5-V maximum, i.e., $2^{12} = 2.5$ V. Finally, the digitized signal was routed to an IBM Personal Computer for display and processing. Typically, over 60 data points/s were acquired and averaged.

† Rodriguez et al.[17] tabulated references for the interferometry applications and adaptations for monitoring thin film processes.

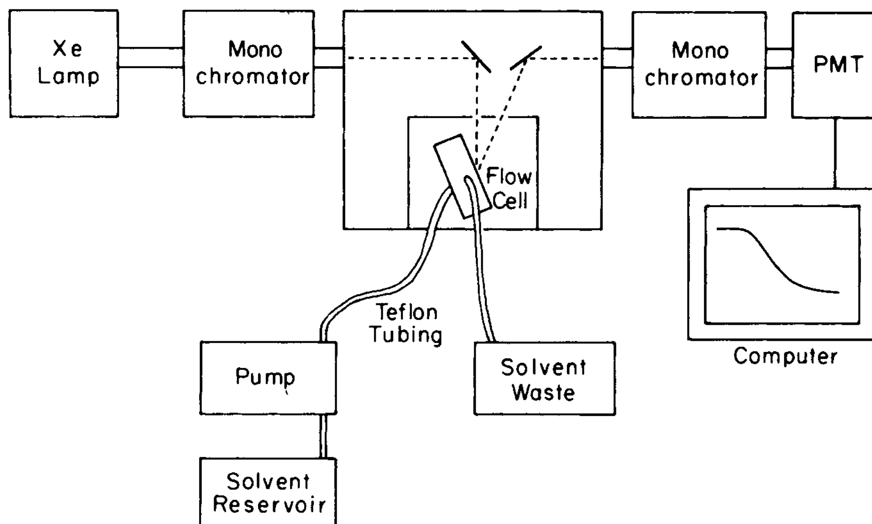

Fig. 3. The experimental setup to monitor fluorescence intensity of a polymer film mounted in the flow cell.

Fluorescence Quenching

Fluorescence intensities were measured with a SPEX FLUOROLOG II spectrometer in the front face (22.5°) geometry. Samples were excited at 290 nm and emission detected at 365 nm. Both excitation and emission slits were set at 0.5 mm. The optical arrangement is illustrated in Figure 3.

RESULTS AND DISCUSSION

Film Thickness Measurement

A Talystep measurement involves the following procedure. A cut on a film sample, to its substrate surface, is made with a razor blade [Fig. 4(A)]. Then, this sample is placed under the Talystep in such a manner so that its stylus scans across the cut. Figure 4(B) is a typical Talystep scan result. Although this technique is normally very accurate, the diamond stylus tends to leave scratch marks on our PMMA film surfaces, which presumably result in an underestimation of the actual film thickness. In our measurement, this procedure was repeated in three different locations each film.

The interferometry method utilizes the optical interference pattern produced due to the change in thickness of a PMMA film during its dissolution. Contrary to the Talystep measurement, there is a danger of overestimation in thickness due to swelling, although PMMA is known for its small degree of swelling during dissolution.[18]

Table I below summarizes the PMMA film thicknesses determined from these two methods. A consistent deviation of ca. 0.1 μm in film thickness for Talystep and interference measurements is attributed to the underestimation of the former and the slight overestimation of the latter.

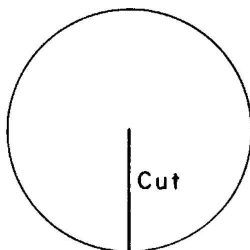

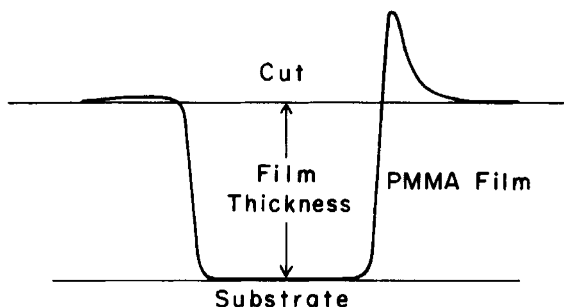

Fig. 4. A Talystep measurement.

TABLE I
Thicknesses of PMMA Films Determined from Talystep and Interferometry

Substrate	Sample	Talystep (μm)	Interferometry (μm)
Quartz	21	0.75 0.75 0.75	0.80
disc	26	0.70 0.75 0.70	0.80
(1/23)	27	0.70 0.70 0.70	0.85
	28	0.75 0.75 0.75	0.85
	31	0.75 0.75 0.70	0.85
	32	0.75 0.70 0.75	0.80
	34	0.70 0.70 0.70	0.85
Silicon			
wafer	5	0.80 0.80 0.80	—
Quartz	12	0.26 0.28 0.28	0.40
disc	13	0.28 0.28	0.40
(12/24)	18	0.27 0.28 0.28	0.40
	19	0.27 0.28 0.28	0.40
	20	0.28 0.29 0.28	—
Silicon	1	0.28 0.28 0.28	0.35
wafer	4	0.28 0.28 0.30	0.35
	8	0.28 0.30 0.28	0.40

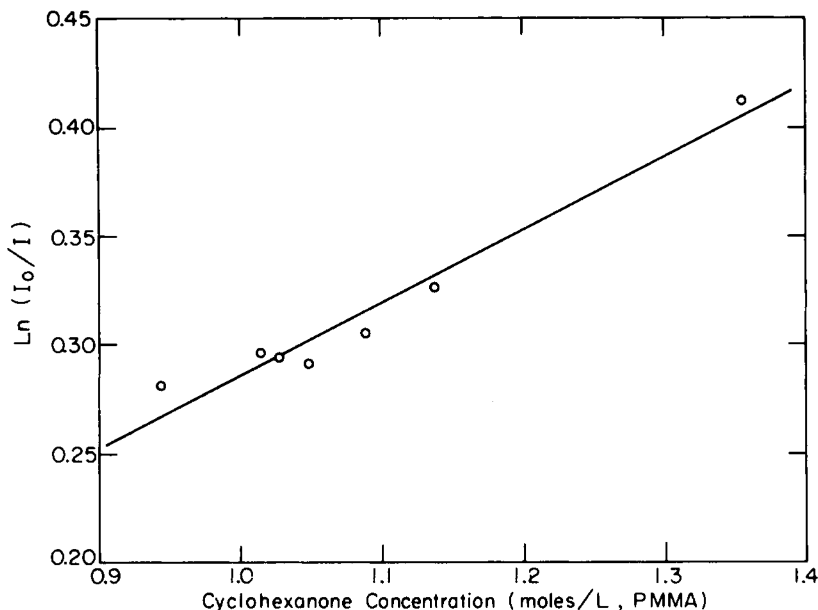

Fig. 5. A semilogarithmic plot of I_0/I as a function of the quencher concentration.

Critical Quenching Distance of the Ketone–Phenanthrene System

Although much of the cyclohexanone in the spin solution is lost upon spin-coating and baking, films containing upward of 20% cyclohexanone by weight can be prepared by limiting the bake period to 5 min at 115°C. This concentration of ketone quenches a significant amount of phenanthrene fluorescence. Fluorescence intensity measurements were corrected for the very small competing light absorption by the ketone at 290 nm, and the data were plotted according to eq. (1) (Fig. 5). The slope of the plot $(4\pi N_A R_0^3/3)$, has the value $0.29M^{-1}$, from which we calculate a critical interaction distance of $R_0 = 4.9$ Å.

Dissolution of PMMA Films Spun on Silicon Wafers

Figure 6 shows an interferometer trace of a PMMA film spun on a silicon wafer. The abrupt fall and the rise of the intensity shown initially are due to the solvent entering the flow cell cavity. The ensuing sinusoidal waveform indicates that the thickness of the PMMA film is changing, i.e., it is dissolving. The final baseline intensity is due to light reflection from the solvent–substrate interface since the PMMA film has been completely dissolved. The baseline prior to the introduction of solvent into the flow cell is higher than the final baseline. This is due to the decrease in the reflectivity at the sample end of the fiber-optic cable as the solvent replaces air in the flow cell. Since the index of refraction of the fiber-optic glass is much closer to that of the solvent than that of the air, the reflection of the laser beam is reduced at the fiber-optic/solvent interface.

Between the initial and the final baselines, the trace shows several salient features. First, only one sinusoidal waveform is visible. This points to two

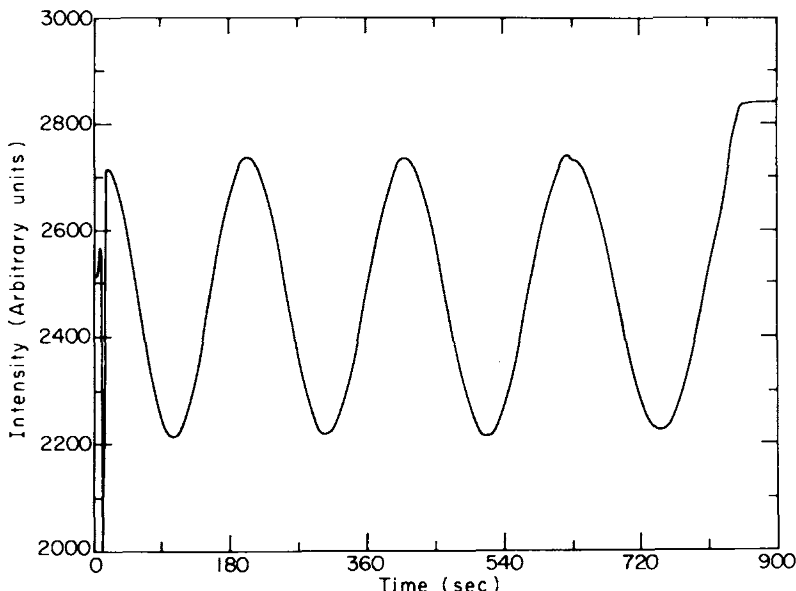

Fig. 6. Interference trace of a PMMA film spun on a silicon wafer (annealed at 160°C for 1 h, solvent = 1 : 1 MEK/IPA).

possibilities. One of these is that a single optical boundary exists between the solvent and PMMA film. The other is that multiple boundaries are present, which all move at the same speed. If the boundaries were moving at varying speeds, a "bumpy" sine curve would be observed.

Secondly, the period of the oscillation remains virtually constant. This indicates that the PMMA film dissolves at a constant rate in the 1 : 1 MEK/IPA mixture. Thirdly, the maxima of the interferometer traces are slightly lower in intensity than the final baseline. This "offset" is attributed to two factors. One of these is the effect of averaging slight variations in film thickness. These arise from differences in the extent of the solvent-front penetration into the PMMA matrix and from variation in the original thickness of the film. The second factor is an intensity reduction due to reflection from a diffuse interface, the transition layer.[17] The fact that the magnitudes of offset vary little among a batch of PMMA films indicates that the first factor is negligible.

Another feature is the remarkable stability of the oscillation amplitude. This indicates that the advance of the solvent front is fairly uniform throughout the region monitored by the He–Ne laser. In other words, the solvent penetration follows the relaxation-controlled mechanism. If the solvent diffusion followed the Fickian model, one would observe an interference pattern with gradually decreasing amplitude.

Figure 7 shows the process of PMMA film dissolution. The data points represent the positions of extrema in Figure 6, which provide the average thicknesses of film remaining at those times. The slope of the plot is virtually linear except for a slight positive deviation from linearity at the onset of the dissolution process. The dissolution rates of Phe-labeled PMMA films and nonlabeled PMMA films were essentially identical.

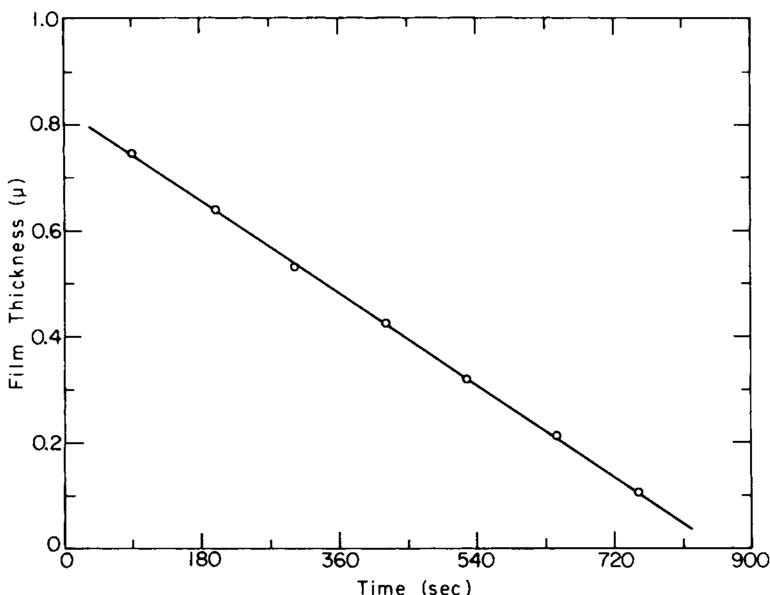

Fig. 7. A film thickness vs. time plot using the results from Figure 6.

Reflectivity of Transition Layer

The thickness of transition layer can be estimated by comparing the reflectivity obtained from the offset of interference trace and that calculated from an optical equation as a function of film thickness. The offset results primarily from the finite thickness of transition layer, which reduces the amount of light reflected. Therefore, the reflectivity of transition layer is estimated from the interference trace assuming that the final baseline represents the reflectivity of a sharp solvent–silicon interface.

In order to calculate the reflectivity of a transition layer, a profile of refractive index across it must be known. Since this information is not readily available, we rely on the solvent concentration gradient model proposed by Crank.[19] Since the relationship between the refractive index and solvent concentration within a polymer–solvent system is linear, one is justified in borrowing Crank's profile for the reflectivity calculation. As a convenient approximation to the Crank's profile, which he presented pictorially, we use a cosine function (Fig. 8).

Given a shape of a refractive index profile between two continuous media of refractive indices n_1 and n_2, the reflectivity of transition layer can be calculated exactly.[20] This method involves slicing the transition layer into infinitesimally thin slices, calculating matrix elements associated with each slice, and, finally, determining the total reflectivity of the transition layer. For each thin slice, we define a transfer matrix M:

$$M = \begin{vmatrix} \cos kl & -(i/n)\sin kl \\ -in\sin kl & \cos kl \end{vmatrix} \tag{6}$$

where n is the refractive index of the slice, l is the thickness of the slice, and

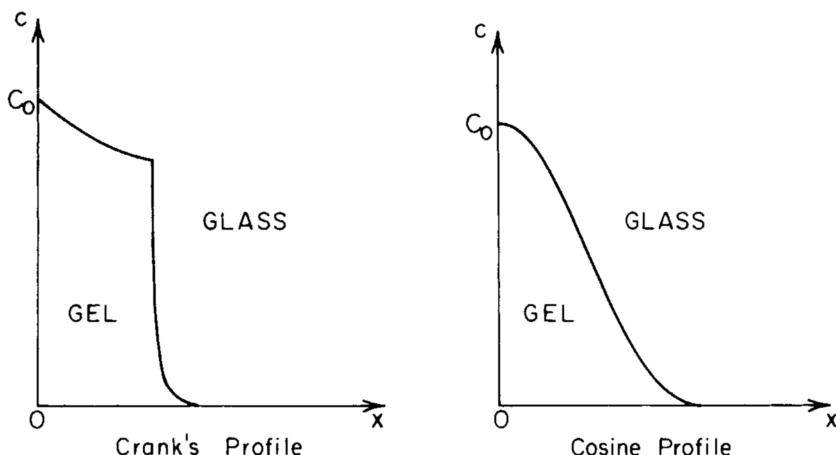

Fig. 8. Crank's concentration profile[19] and cosine profile of solvent penetrating into a glassy polymer.

$k = 2\pi/\lambda = 2\pi n/\lambda_0$. Then, the transfer matrix elements of the whole transition layer are

$$M_1 M_2 M_3 \cdots M_n = \begin{vmatrix} A & B \\ C & D \end{vmatrix} \tag{7}$$

The reflectivity R equals $|r|^2$, where

$$r = \frac{An_1 + Bn_1n_2 - C - Dn_2}{An_1 + Bn_1n_2 + C + Dn_2} \tag{8}$$

This calculation is repeated for transition layers of various thicknesses, and the relationship is plotted (Fig. 9). Finally, one can associate the reflectivity of transition layer estimated from the interference trace with its physical thickness.

From the magnitude of the offset in the interference trace of Figure 6, we calculate a thickness of 92 nm in this manner. The profile drawn by Crank is steeper than the cosine profile. A steeper solvent concentration profile with a similar offset value would imply a thicker transition layer.

Dissolution of PMMA Films Spun on Quartz Discs

The index of refraction of fused quartz (1.458) is quite close to that of PMMA (1.489). Consequently, the reflectivity at this interface is very weak, $R_2 = 1.1 \times 10^{-5}$. However, unlike the silicon wafer substrate, the quartz discs are transparent to the He–Ne laser beam. This generates an additional optical interface at the quartz/air boundary. At this interface, $R_3 = 3.472 \times 10^{-2}$, more than three orders of magnitude larger than R_2. Therefore, R_3 and R_1 will be the major contributors to the observed interference trace. Furthermore, since the double optical thickness of the quartz disc is not necessarily an integer multiple of the wavelength of the He–Ne laser, unlike the silicon wafer

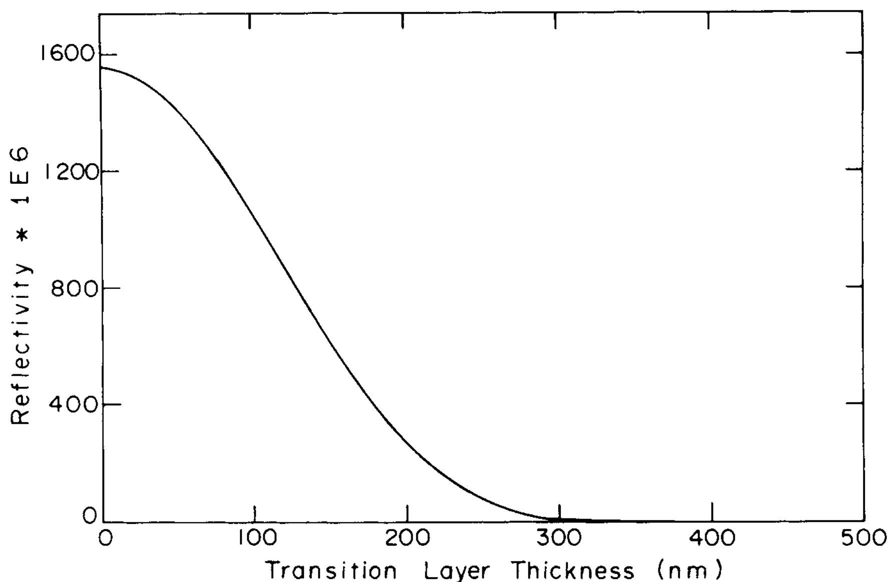

Fig. 9. Calculated reflectivity as a function of the transition layer thickness using a cosine concentration profile.

films, the final baseline would not necessarily settle above the interference maxima. Figure 10 shows that the final baseline lies below the interference maxima. The relative position of the baseline upon completion of dissolution is the same for all our samples spun on quartz substrates, which implies that these discs must have remarkably similar thicknesses.

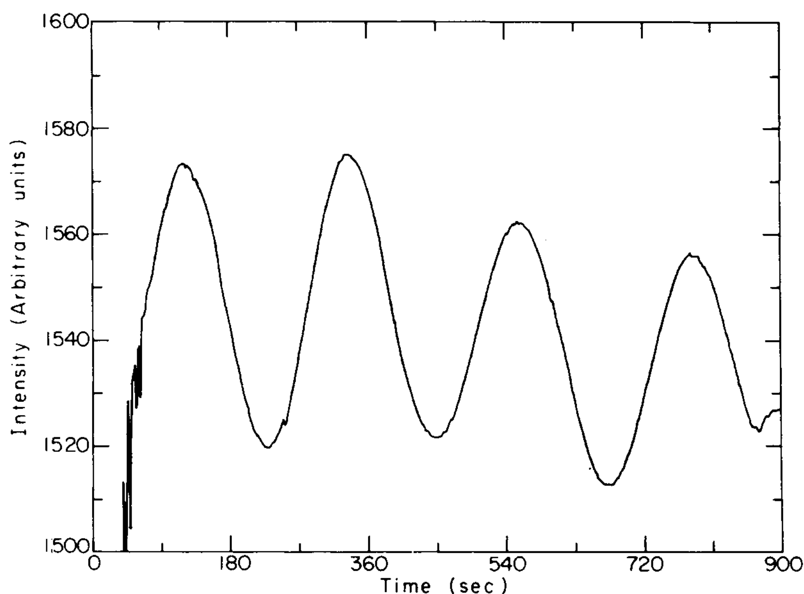

Fig. 10. Interference trace of a PMMA film spun on a quartz disc as a function of exposure time to solvent (annealed at 160°C for 1 h, solvent = 1 : 1 MEK/IPA).

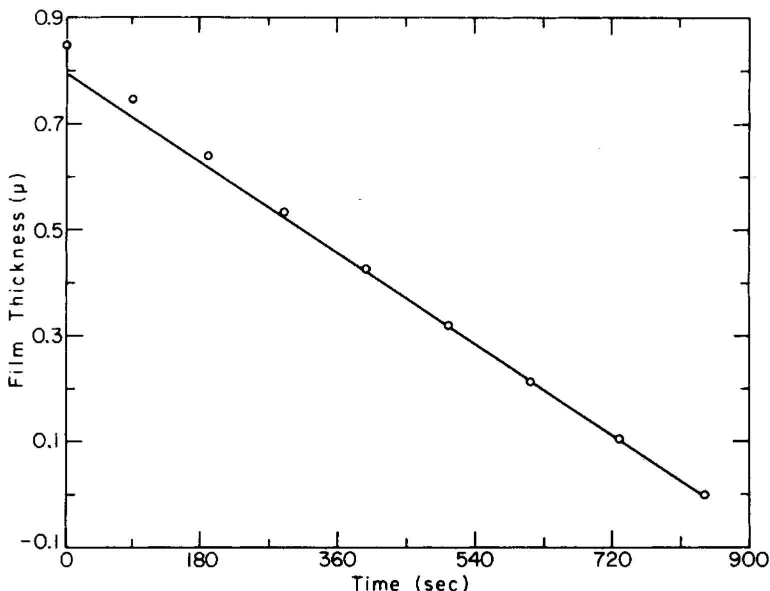

Fig. 11. A film thickness vs. time plot using the results from Figure 10.

The film dissolution rate calculated from the data in Figure 10 is shown in Figure 11, which is identical to Figure 7. Here and in our other experiments, the substrate upon which the PMMA film is spun seems to make little difference in the thickness of film prepared or in its dissolution rate.

Solvent Penetration

Figure 12 shows the decay in fluorescence intensity of phenanthrene labels on the PMMA backbone caused by exposing the film to flowing solvent. This fluorescence signal can be divided into three parts for analysis. The first part represents the presolvent contact stage. The baseline is quite stable here.

The second section starts with a rather abrupt drop in fluorescence intensity. This signals the onset of solvent–PMMA contact. This contact period is extended in time due to the height of the excitation beam (ca. 5 mm) coupled with a slow solvent pumping speed used for this experiment (ca. 10 s to fill up the cell cavity). The reduction in fluorescence intensity during the contact period is due to at least two factors. The obvious one is the MEK quenching of the fluorescence of solvent-exposed phenanthrene, which accounts for ca. 0.1% of the total fluorescence intensity assuming $R_0 = 5$ Å and a total film thickness of 0.8 μm. The other factor is the reduced reflectivity at the PMMA/solvent interface. This is responsible for a ca. 4% reduction of the measured fluorescence intensity. After the initial solvent–PMMA contact, the rate of fluorescence decay accelerates slightly. This implies an increase in penetration rate due to plasticization. The penetration rate stabilizes gradually, yielding a linear decay of fluorescence in time. This is the mark of a relaxation-controlled diffusion, consistent with the inferences made from the interferometer trace analysis.

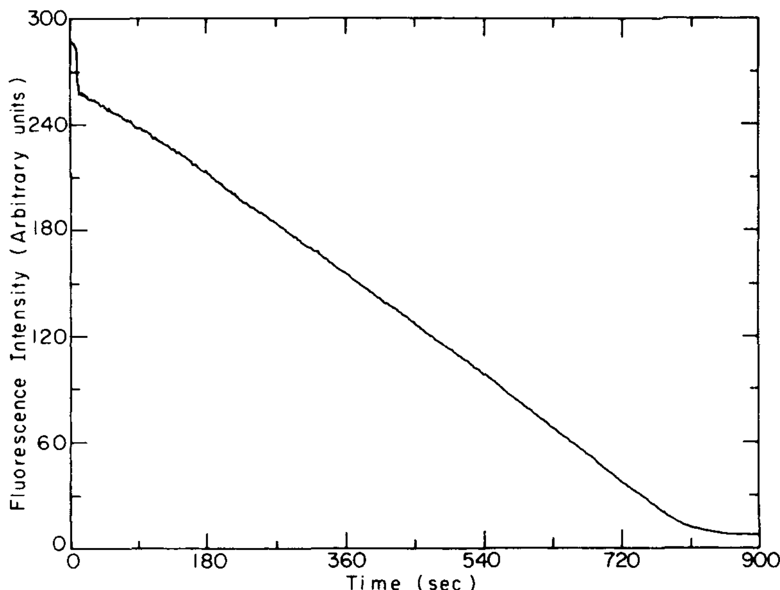

Fig. 12. Decay of fluorescence intensity from a phenanthrene-labeled PMMA film as a function of the time it is exposed to solvent (measured simultaneously with the results shown in Fig. 10).

The last part starts with a positive deviation from the linearity (ca. 800 s). This would occur, for example, if a decrease in the solvent penetration rate occurred. Then, a continued decay in fluorescence with a different slope would be expected. However, we have no reason to expect a reduction in penetration rate far ahead of the completion of the dissolution process, independent of film thickness. A more plausible explanation for this deviation is that the concentration of excited chromophores available for immediate quenching is decreasing. This can be brought about by the vangard MEK vapor reaching the substrate surface. Then, the slower quenching rate observed could be due to two factors: (i) the continual increase in MEK concentration at the quartz surface leading to lower quenching rate per MEK molecule and (ii) the difficulty in quenching some Phe labels of PMMA molecules adhered to the quartz surface. The latter is not unreasonable since MEK quenches Phe by a short-range energy transfer mechanism.

Finally, the fluorescence intensity stabilizes to a declining baseline, consisting of a moderate fluorescence intensity from solvated PMMA–Phe which are slowly exiting the flow cell as well as a nominal intensity from the scattered radiation.

Comparison of Solvent Diffusion and Polymer Dissolution

In Figure 13 we present the time profile of the dissolution measurement obtained by laser interferometry superposed with the simultaneous measure of fluorescence intensity decay. The onset of dissolution is ca. 50 s delayed with respect to the solvent–PMMA contact, which appears in the fluorescence trace as a sudden sharp decrease in intensity. This delay reflects the time

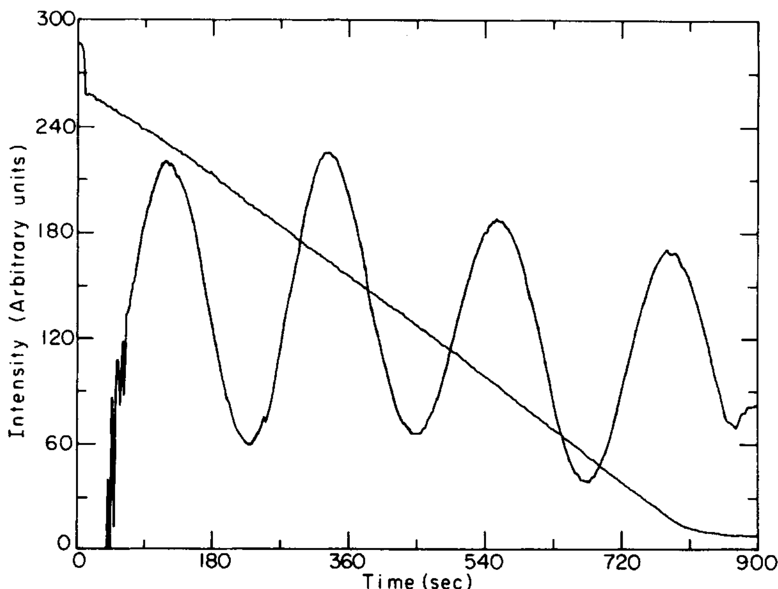

Fig. 13. A superimposed image of Figures 10 and 12.

necessary to form a *nascent* transition layer that includes a solvent-swollen gel layer from which polymer chains diffuse into solution. The first experimental evidence for the existence of the transition layer in PMMA film dissolution was recently reported by Krasicky et al.[21] Through careful oblique-angle laser interferometry experiments, they established the existence of two reflecting boundaries associated with film dissolution and calculated its thickness to be 86 nm. It is natural to assume that one boundary is that between the solvent front and the solvent-free PMMA matrix, and the other is the outermost point in the swollen gel layer where the laser beam is effectively reflected.

At the end of the process, the completion of dissolution is about 90 s delayed with respect to the solvent front reaching the quartz substrate. This is the time thickness of the *steady state* transition layer. We use this value in conjunction with the dissolution rate (1.0 nm/s) measured by laser interferometry to obtain 90 nm as the thickness of the transition layer. This is in good agreement with the 92 nm thickness calculated from reflectivity of the transition layer using a cosine concentration profile. In addition, this value compares well with that reported by Krasicky et al.[21] Although their value was obtained with pure MEK as the solvent, deviation from this value for 1 : 1 MEK/IPA mixture should be small, since they found that a change in solvent has little effect on the thickness of transition layer as long as good solvents are used.[21]

Further insights into the dissolution mechanism can be obtained by superposing plots of the time profile of film dissolution with that of the fluorescence intensity decay (Fig. 14). The small "auto-acceleration" observed during the plasticization stage in the fluorescence trace has no counterpart in the loss of material from the film, which remains linear throughout this region. We attribute these changes to a growth in the thickness of the transition layer from 50 to 90 nm. Subsequently, the slope of the fluorescence decay and that

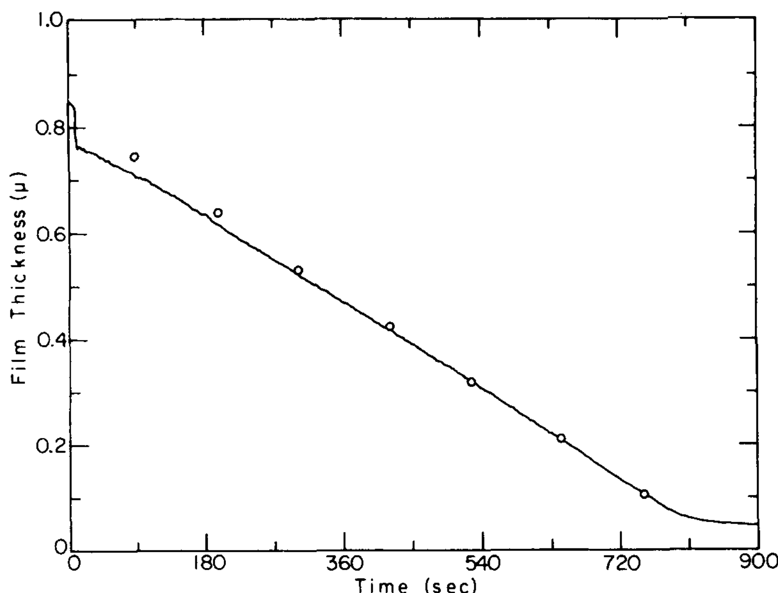

Fig. 14. A superimposed image of Figures 11 and 12.

of the decrease in film thickness coincide. This indicates that the thickness of the transition layer remains constant throughout the remainder of the dissolution process.

CONCLUSION

Photoresist dissolution is an important aspect of integrated circuit fabrication. A novel experimental method based upon fluorescence measurements enables us to monitor simultaneously the rate of solvent penetration into a PMMA film and its dissolution.

Our initial results show that 1 : 1 MEK/IPA solvent mixture penetrates into PMMA films annealed at 160°C via the relaxation-controlled diffusion mechanism. Consequently, once the steady state is reached, the solvent penetration rate determines the photoresist dissolution rate.

The thickness of the steady-state transition layer has been determined to be ca. 90 nm by this new technique. This value is in good agreement with the thickness calculated from the reflectivity of the transition layer. In addition, the thickness of the transition layer increases from 50 to 90 nm exclusively during the plasticization stage.

The authors wish to thank NSERC Canada and the IBM SUR program for their support of this research as well as Xerox Canada for the use of the Talystep instrument there.

References

1. C. G. Willson, in *Introduction to Microlithography*, L. F. Thompson, C. G. Willson, and M. J. Bowden, Eds., ACS Symposium Ser. 219, Am. Chem. Soc., Washington, DC, 1983.

2. A. C. Ouano, Y. O. Tu, and J. A. Carothers, in *Structure–Solubility Relationship in Polymers*, F. W. Harris and R. B. Seymour, Eds., Academic, New York (1977).

3. A. C. Ouano, *Polym. Eng. Sci.*, **18**(4), 306 (1978); *Polymers in Electronics*, ACS Symp. Ser. 242, T. Davidson, Ed., Am. Chem. Soc., Washington, DC, 1984.

4. A. C. Ouano and J. A. Carothers, *Polym. Eng. Sci.*, **20**(2), 160 (1980).

5. J. Crank, *The Mathematics of Diffusion*, Clarendon, Oxford, 1975.

6. T. Alfrey, E. F. Gurney, and W. G. Lloyd, *J. Polym. Sci.*, **C12**, 249 (1966).

7. N. Thomas and A. H. Windle, *Polymer*, **19**, 255 (1978).

8. T. J. Lewis, *Polymer*, **19**(3), 285 (1978).

9. K. Ueberreiter, in *Diffusion in Polymers*, J. Crank and G. S. Park, Eds., Academic, New York, 1968.

10. S. Tazuke and M. A. Winnik, in *Photophysical and Photochemical Tools in Polymer Science*, M. A. Winnik, Ed., NATO ASI Series C, Vol. 182, Reidel, Dordrecht, Netherlands, 1986.

11. J. B. Birks, *Photophysics of Aromatic Molecules*, Wiley-Interscience, New York, 1970, p. 434.

12. F. Perrin, *C. R. Acad. Sci. Paris*, **178**, 1978 (1924); *Ann. Chem. Phys.*, **17**, 283 (1932).

13. M. Inokuti and F. Hirayama, *J. Chem. Phys.*, **43**, 1978 (1965).

14. J. B. Birks, *Photophysics of Aromatic Molecules*, Wiley-Interscience, New York, 1970, p. 443.

15. *Polymer Handbook*, 2nd ed., J. Brandrup and E. H. Immergut, Eds., Wiley-Interscience, New York, 1975, p. III–148.

16. D. Stanton, M.S. thesis, University of Toronto, 1985, pp. 56–63.

17. F. Rodriguez, P. D. Krasicky, and R. J. Groele, *Solid State Technol.*, **28**, 125 (May 1985).

18. *Polymer Handbook*, 2nd ed., J. Brandrup and E. H. Immergut, Eds., Wiley-Interscience, New York, 1975, p. III–242.

19. J. Crank, *J. Polym. Sci.*, **11**, 151 (1953).

20. G. R. Fowles, *Introduction to Modern Optics*, Holt-Reinhart-Winston, Toronto, 1975, pp. 96–98.

21. P. D. Krasicky, R. J. Groele, J. A. Jubinsky, F. Rodriguez, Y. M. N. Namaste, and S. K. Obendorf, *Polym. Eng. Sci.*, **27**(4), 282 (1987).

Received September 11, 1987
Accepted September 21, 1987